

# Ultrathin Pt–Cu–Ni Ternary Alloy Nanowires with Multimetallic Interplay for Boosted Methanol Oxidation Activity

Zhixue Zhang,<sup>§</sup> Miao Xie,<sup>§</sup> Zhaojun Liu, Yiming Lu, Shumeng Zhang, Moxuan Liu, Kai Liu, Tao Cheng,<sup>\*</sup> and Chuanbo Gao<sup>\*</sup>



Cite This: *ACS Appl. Energy Mater.* 2021, 4, 6824–6832



Read Online

ACCESS |

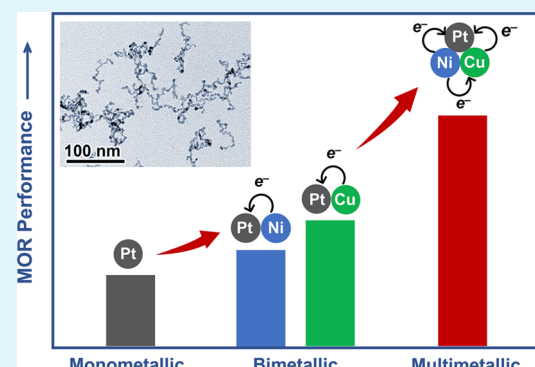
Metrics & More

Article Recommendations

Supporting Information

**ABSTRACT:** Controllably incorporating multiple non-noble metals into noble metal nanoparticles may greatly extend the degree to which the electronic structure and thus the catalytic activity of the nanoparticles could be engineered, which suffers from ineffective coreduction of metals with different reduction potentials. In this work, we achieved the designable synthesis of such multimetallic alloy nanomaterials exemplified by ultrathin Pt–Cu–Ni ternary alloy nanowires by involving an electroless plating mechanism. Experiments and density functional theory (DFT) calculations show remarkable electronic coupling among the multiple alloy components. As a result, the Pt–Cu–Ni ternary alloy possesses a higher adsorption energy of \*OH and a lower adsorption energy of \*CO than any of the Pt–M (M = Cu, Ni) binary alloys, both being favorable for boosting the kinetics of the methanol oxidation reaction (MOR). The specific and mass activities of the ternary alloy nanowires well surpass those of the binary alloy counterparts and reach up to  $7.4 \text{ mA cm}^{-2}$  and  $2.1 \text{ A mg}_{\text{Pt}}^{-1}$ , respectively, making them top-ranked catalysts. The multimetallic electronic coupling further makes Cu, the major non-noble metal component, less prone to leaching, leading to improved stability. Our results showcase the intriguing catalytic properties by modifying the electronic structure of noble metal nanoparticles by multiple non-noble metal alloy components, which opens up opportunities in the design of highly efficient catalysts for the MOR and many other applications.

**KEYWORDS:** noble metal nanoparticles, nanowires, ultrasmall thickness, Pt–Cu–Ni ternary alloy, multimetallic interplay, methanol oxidation reaction



## INTRODUCTION

Pursuing highly efficient electrocatalysts for the methanol oxidation reaction (MOR) is central to the development of direct methanol fuel cell technology for the power supply of portable devices and vehicles.<sup>1,2</sup> Among different metals, Pt stands out because of its high capability of activating methanol. However, the methanol oxidation reaction is a kinetically sluggish process due to the poisoning of the Pt catalysts by the CO intermediate.<sup>3–5</sup> As alloying is a widely recognized strategy to improve the catalytic properties,<sup>6–10</sup> Pt–M (M: second metal) alloy nanoparticles are often employed in this catalysis to facilitate the oxidation of the CO intermediate. The metal for the alloying could be an oxophilic noble metal such as Ru, which readily affords surface M–OH species as an oxidizing agent for the oxidation of the CO intermediate.<sup>11–17</sup> Non-noble metals, Cu, Ni, Bi, and Sn, for example, are excellent alternatives of the alloy components because they can effectively modify the electronic structure of Pt and weaken the adsorption energy of CO at the Pt sites for its convenient oxidation.<sup>18–29</sup> The use of non-noble metals further reduces the cost of the catalyst. So far, the alloy catalysts for the MOR usually contain a single non-noble metal as the electronic

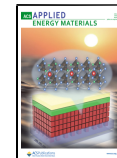
modifier, which significantly limits the extent to which the electronic structure of Pt could be modulated.<sup>30,31</sup> We anticipate that alloying Pt with multiple non-noble metals may cause significant electronic coupling among the multiple metals,<sup>32</sup> affording interesting catalytic properties that are distinct from those of the alloy nanoparticles with a single non-noble metal component. However, such an effect has not been revealed in the electrocatalytic MOR. Few prior works have manifested mutual interplay between the multimetallic components for boosted methanol oxidation activity, to the best of our knowledge.

A significant obstacle to the investigation of the interplay between Pt and multiple non-noble metals lies in the synthesis. Due to the huge gaps between the reduction potentials of different metal salts, the metals are usually reduced at quite

Received: March 31, 2021

Accepted: June 23, 2021

Published: July 7, 2021



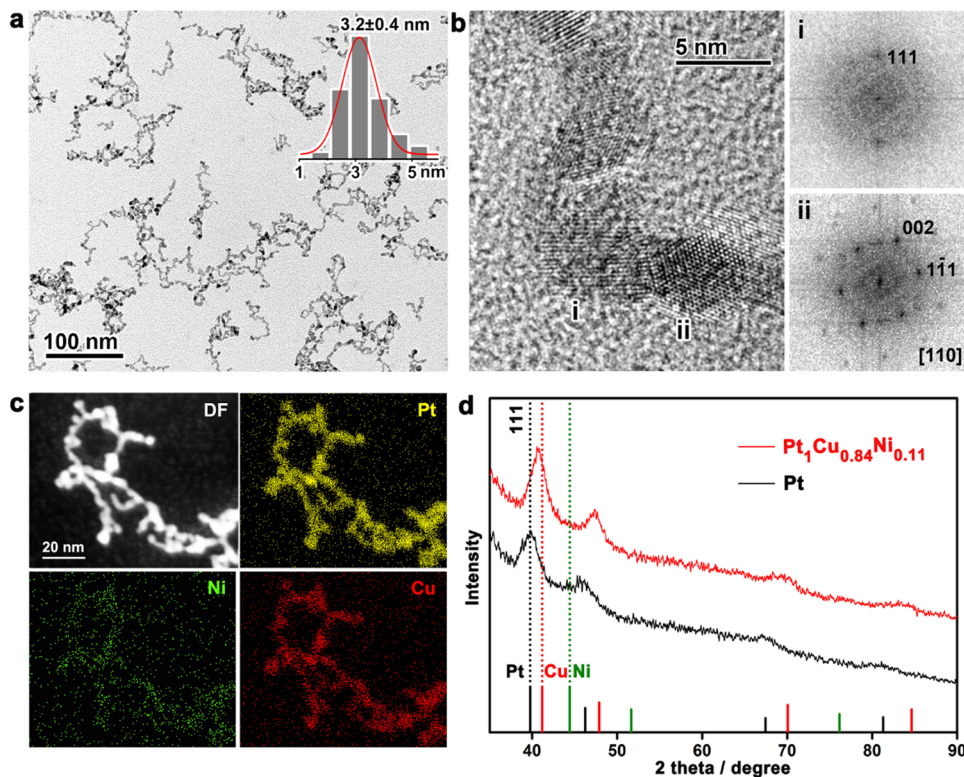


**Figure 1.** Characterizations of the ultrathin  $\text{Pt}_1\text{Cu}_{0.84}\text{Ni}_{0.11}$  ternary alloy nanowires. (a) TEM image. Inset shows the diameter histogram of the nanowires. The average diameter was expressed as “mean  $\pm$  standard deviation.” (b) HRTEM image. Right to the image: Fourier diffractograms of the zones are labeled as (i) and (ii). (c) Elemental mapping by EDS. (d) XRD patterns of the ultrathin  $\text{Pt}_1\text{Cu}_{0.84}\text{Ni}_{0.11}$  nanowires and monometallic Pt nanowires. Black, red, and green sticks indicate the peak positions of pure Pt, Cu, and Ni, respectively.

different rates, making it difficult to synthesize multimetallic alloy nanoparticles in a controllable manner.<sup>33,34</sup> Therefore, such multimetallic alloy nanoparticles are generally synthesized by impregnation,<sup>35,36</sup> galvanic replacement reaction,<sup>37</sup> one-pot coreduction of multiple metal salts with a large excess of non-noble metal ingredients,<sup>38–42</sup> and doping a third non-noble metal into pre-existing noble metal/non-noble metal alloy nanoparticles,<sup>43–46</sup> showing difficulty in achieving homogeneity and tunability in the alloy composition and the particle size. Our previous work suggests that the huge gap between the reduction potentials of two metal salts could be remedied by introducing inorganic ligands,  $\text{SO}_3^{2-}$ , for example, into the wet-chemical synthesis.<sup>47</sup> Activated hydrogen was assumed to form via an electroless plating mechanism, which favors the effective coreduction of the metal salts to form noble metal/non-noble metal binary alloy nanoparticles. We anticipate that this strategy may provide the opportunity to alloy multiple non-noble metals in Pt nanoparticles with high controllability and, therefore, pave the way to the exploration of their intriguing catalytic properties.

In this work, we report a successful synthesis of Pt–Cu–Ni ternary alloy nanowires with an ultrasmall thickness ( $\sim 3.2$  nm) and broadly tunable compositions by introducing an electroless plating mechanism into a wet-chemical hydrothermal system, and based on this synthesis, reveal the clear existence of an interesting interplay between Pt and the multiple non-noble metals for improved activity and stability in the electrocatalytic MOR. By finely tuning the ternary alloy compositions, a high specific activity of  $7.4 \text{ mA cm}^{-2}$  and a mass activity of  $2.1 \text{ A mg}_{\text{Pt}}^{-1}$  have been achieved in  $1 \text{ M } \text{CH}_3\text{OH} + 0.5 \text{ M } \text{H}_2\text{SO}_4$ . Notably, the specific activities were 1.8 and 2.4 times greater

than those of Pt–Cu and Pt–Ni binary alloy nanowires, respectively, which confirms the role of the multimetallic interplay in improving the activity of the catalyst toward the methanol oxidation reaction. A density functional theory (DFT) calculation reveals the electron redistribution among the ternary components and thereby distinctive electronic properties: although the ternary alloy nanowires bind  $^*\text{OH}$  more strongly, they bind  $^*\text{CO}$  more weakly than any of the binary alloy catalysts, favorable for accelerating the methanol oxidation kinetics. The electronic coupling also increases the formation energy of Cu vacancy on the ternary alloy surface and thus decreases the leaching rate of Cu, the major non-noble metal component, from the catalyst, which leads to improved stability of the catalysts. We believe the synthetic chemistry and the multimetallic interplay revealed in this work open an avenue to a family of multimetallic alloy catalysts for sustainable energy and many other applications.

## RESULTS AND DISCUSSION

**Synthesis and Characterization.** In a typical synthesis of the Pt–Cu–Ni ternary alloy nanowires, the metal salts of  $\text{H}_2\text{PtCl}_6$ ,  $\text{CuCl}_2$ , and  $\text{NiCl}_2$  were dissolved in ethylene glycol (EG) in the presence of poly(vinylpyrrolidone) (PVP),  $\text{Na}_2\text{SO}_3$ , and formic acid (HCOOH). Among these chemicals, PVP serves as a surfactant to render the alloy nanoparticles with colloidal dispersity,  $\text{Na}_2\text{SO}_3$  was employed to induce the electroless plating mechanism and overcome the reduction potential difference of the metal salts,<sup>47</sup> and HCOOH was used to adjust the pH. The reaction system was sealed in a Teflon-lined stainless steel autoclave and heated at  $205^\circ\text{C}$  for 6 h. The solid product was collected by centrifugation and

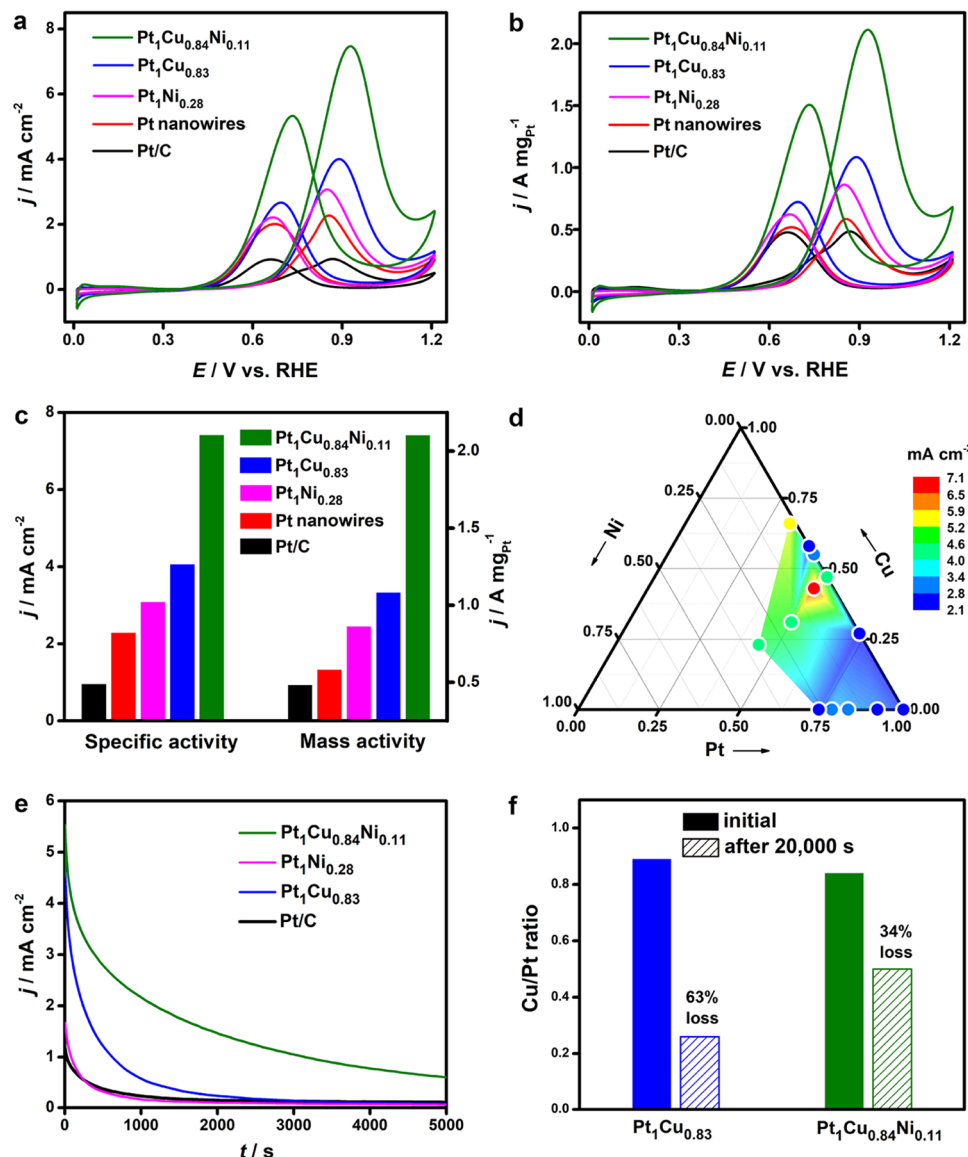


**Figure 2.** Electrocatalytic methanol oxidation performance of the Pt–Cu–Ni ternary alloy nanowires compared with those of the Pt–Cu and the Pt–Ni binary alloy nanowires. (a, b) CV curves of the electrocatalysts in 0.5 M  $\text{H}_2\text{SO}_4$  + 1 M  $\text{CH}_3\text{OH}$  at a scan rate of 50  $\text{mV s}^{-1}$ . The current densities are normalized to the ECSA (a) and the mass of Pt (b), respectively. (c) Comparison of the specific and mass activities of catalysis at the peak position. (d) Diagram of the specific activities of the alloy nanowires in the MOR. Different colors represent the activity values. The colors in between data points are for eye guidance. (e) Chronoamperometric  $i$ – $t$  curves of the catalysts at 0.8 V vs a reversible hydrogen electrode (RHE) in 0.5 M  $\text{H}_2\text{SO}_4$  + 1 M  $\text{CH}_3\text{OH}$ ; (f) change of the Cu/Pt ratio in the  $\text{Pt}_1\text{Cu}_{0.84}\text{Ni}_{0.11}$  and  $\text{Pt}_1\text{Cu}_{0.83}$  alloy nanowires during the chronoamperometric  $i$ – $t$  test.

washed with  $\text{H}_2\text{O}$ . As shown in the transmission electron microscopy (TEM) image, ultrathin nanowires have been obtained from this synthesis in a high yield (Figure 1a). The average diameter of the nanowires was measured to be  $3.2 \pm 0.4$  nm. The high-resolution TEM (HRTEM) image and corresponding Fourier diffractograms suggest that the nanowires are polycrystalline with lattice orientations varying from site to site through the whole nanowires (Figure 1b). This suggests that the nanowires were formed by one-dimensional attachment of primary nanoparticles rather than the crystal growth from individual nuclei. The composition of the nanowires obtained from a typical synthesis ( $\text{Pt}/\text{Cu}/\text{Ni} = 1:1:1$  in the precursor) was measured to be  $\text{Pt}_1\text{Cu}_{0.84}\text{Ni}_{0.11}$  ( $\text{Pt}/\text{Cu}/\text{Ni} = 1:0.84:0.11$ ) by inductively coupled plasma mass spectrometry (ICP-MS), which confirms the effective

coreduction of metal salts to form a ternary alloy. These metallic components were homogeneously distributed in the nanowires, as revealed by the energy-dispersive X-ray spectroscopy (EDS) elemental mapping (Figure 1c). The X-ray diffraction (XRD) peaks of the nanowires can be indexed as 111, 200, 220, and 222 reflections of a face-centered cubic (fcc) lattice (Figure 1d). The peaks shift systematically to higher  $2\theta$  values than monometallic Pt, in line with a shrinkage of the lattice size due to the Pt–Cu–Ni alloying. The lattice shrinkage can also be verified by HRTEM (Figure S1). Compared with the {111} spacing of 2.27 Å in pure Pt, the {111} spacing in the nanowires was measured to be 2.24 Å, again confirming the alloying of Pt with non-noble metals of Cu and Ni in the nanowires.

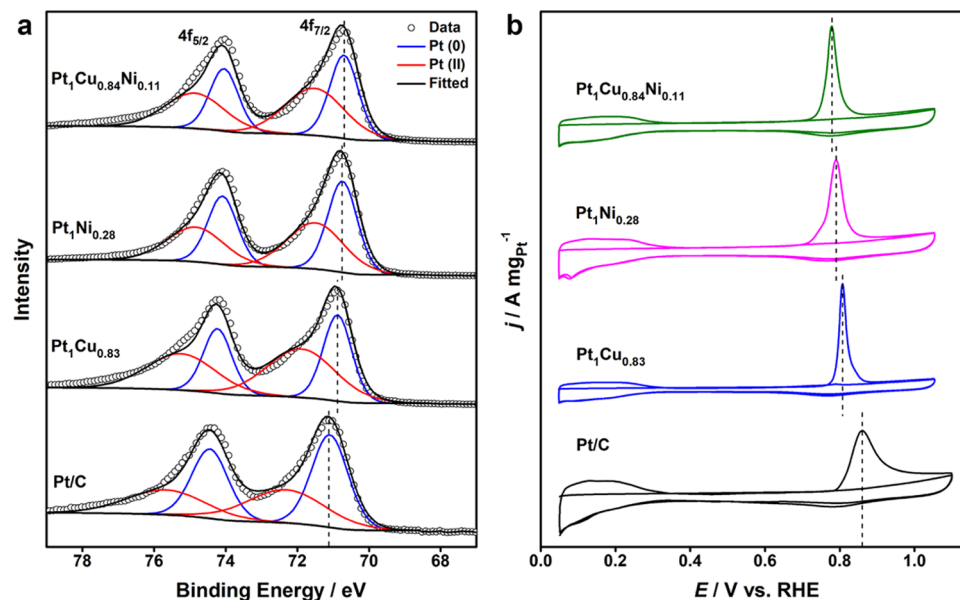


**Figure 3.** Characterization of the electronic properties of the Pt–Cu–Ni, Pt–Cu, Pt–Ni alloy nanowires, and the commercial Pt/C. (a) Pt 4f XPS spectra of the catalysts fitted by 4f<sub>7/2</sub> and 4f<sub>5/2</sub> components. Dashed lines indicate the positions of the Pt(0) 4f<sub>7/2</sub> peaks. (b) CO stripping curves of the catalysts. Dashed lines indicate the positions of the CO oxidation peaks.

Sulfite plays a critical role in the formation of the ultrathin Pt–Cu–Ni ternary alloy nanowires. Instead of nanowires, only quasi-spherical nanoparticles can be obtained when Na<sub>2</sub>SO<sub>3</sub> is absent from a typical synthesis (Pt/Cu/Ni = 1:1:1 in the precursor) (Figure S2). The composition of the nanospheres was measured to be Pt<sub>1</sub>Cu<sub>0.50</sub>Ni<sub>0.02</sub> by ICP-MS (Figure S3). The product already contains a certain fraction of Cu, which can be attributed to the underpotential deposition of Cu<sup>2+</sup> on the Pt nuclei and thus its autocatalytic reduction in the synthesis.<sup>48–50</sup> However, only a trace amount of Ni could be detected in the product, suggesting that the reduction of Ni<sup>2+</sup> is much more difficult in the absence of SO<sub>3</sub><sup>2-</sup>. The SO<sub>3</sub><sup>2-</sup>-assisted wet-chemical synthesis thus enabled the reduction of the multiple metal salts via the electroless plating mechanism to afford Pt–Cu–Ni ternary alloy nanowires with significantly improved controllability. The reduction of Pt may also have occurred in the solution via the direct chemical reduction, which led to a higher Pt content in the nanowires than expected according to the feeding ratios. Nevertheless, the alloy compositions of these nanowires could be effectively tuned by adjusting the concentrations of the respective metal salts in the precursor (Figures S4 and S5 and Tables S1–S3), which paves the way to the study of their composition-dependent catalytic properties. It is worth noting that the synthesis of Pt–Cu–Ni ternary alloy nanoparticles has been previously achieved by several methods such as the galvanic replacement reaction<sup>37</sup> and the one-pot reduction.<sup>39–42</sup> The galvanic replacement synthesis may suffer from the difficulty in precisely tuning the alloy compositions, and the one-pot reduction produces alloy nanoparticles with compositional inhomogeneity due to different reduction kinetics of the metals.<sup>39,40</sup> Our strategy provides opportunities to afford Pt–Cu–Ni ternary alloy nanoparticles with improved tunability and homogeneity of the alloy compositions.

**Electrocatalytic Performance.** The electrocatalytic performance of the ultrathin Pt–Cu–Ni ternary alloy nanowires in the MOR was investigated (Figure S6 and Table S4) and compared with that of the ultrathin Pt–M (M = Cu, Ni)

binary alloy nanowires (Figures S7 and S8), the ultrathin monometallic Pt nanowires, and the commercial Pt/C (JM, 20% Pt/XC72R) (Figure 2). Before the electrocatalytic measurements, all of the nanowires were supported on carbon and activated by annealing in H<sub>2</sub> (5 vol %) at 200 °C for 2 h to ensure a clean surface without significantly changing the morphology and composition of the nanowires (Figures S9 and S10 and Table S5). To make a fair comparison, we examined the catalytic activities of the Pt–Cu and the Pt–Ni binary alloy nanowires with different compositions (Cu/Pt = 0.38–1.33; Ni/Pt = 0.09–0.35), among which Pt<sub>1</sub>Cu<sub>0.83</sub> and Pt<sub>1</sub>Ni<sub>0.28</sub> were found to be the best catalysts in the respective series (Figures S11 and S12 and Tables S6 and S7). The composition of the Pt–Cu–Ni ternary alloy nanowires was also broadly tuned, and Pt<sub>1</sub>Cu<sub>0.84</sub>Ni<sub>0.11</sub> was found to possess the highest activity among all compositions investigated (Figure S6). Figure 2a,b shows the cyclic voltammetry (CV) of the Pt<sub>1</sub>Cu<sub>0.84</sub>Ni<sub>0.11</sub>, Pt<sub>1</sub>Cu<sub>0.83</sub>, and Pt<sub>1</sub>Ni<sub>0.28</sub> nanowires, as well as the monometallic Pt nanowires and the commercial Pt/C, in N<sub>2</sub>-saturated 0.5 M H<sub>2</sub>SO<sub>4</sub> + 1 M CH<sub>3</sub>OH. The current densities are normalized to the electrocatalytically active surface area (ECSA, Figure S13) and the mass of Pt, respectively. The specific and mass activities of the catalysts are summarized in Figure 2c. Both the specific and mass activities increase in the order of Pt/C (0.94 mA cm<sup>-2</sup>, 0.48 A mg<sub>Pt</sub><sup>-1</sup>) < Pt nanowires (2.27 mA cm<sup>-2</sup>, 0.58 A mg<sub>Pt</sub><sup>-1</sup>) < Pt<sub>1</sub>Ni<sub>0.28</sub> nanowires (3.07 mA cm<sup>-2</sup>, 0.86 A mg<sub>Pt</sub><sup>-1</sup>) < Pt<sub>1</sub>Cu<sub>0.83</sub> nanowires (4.05 mA cm<sup>-2</sup>, 1.08 A mg<sub>Pt</sub><sup>-1</sup>) < Pt<sub>1</sub>Cu<sub>0.84</sub>Ni<sub>0.11</sub> nanowires (7.40 mA cm<sup>-2</sup>, 2.10 A mg<sub>Pt</sub><sup>-1</sup>). It is inferred that the Pt–M (M = Ni, Cu) binary alloy nanowires already showed better activities than the monometallic Pt, thanks to the synergy between the binary alloy components. Interestingly, the Pt–Cu–Ni ternary alloy nanowires outperformed these binary alloy nanowires in the MOR. The specific activity of the Pt<sub>1</sub>Cu<sub>0.84</sub>Ni<sub>0.11</sub> ternary alloy nanowires exceeds those of the Pt<sub>1</sub>Ni<sub>0.28</sub> and the Pt<sub>1</sub>Cu<sub>0.83</sub> binary alloy nanowires by factors of 1.8 and 2.4, respectively, which highlights the superiority of multimetallic synergy in boosting the methanol

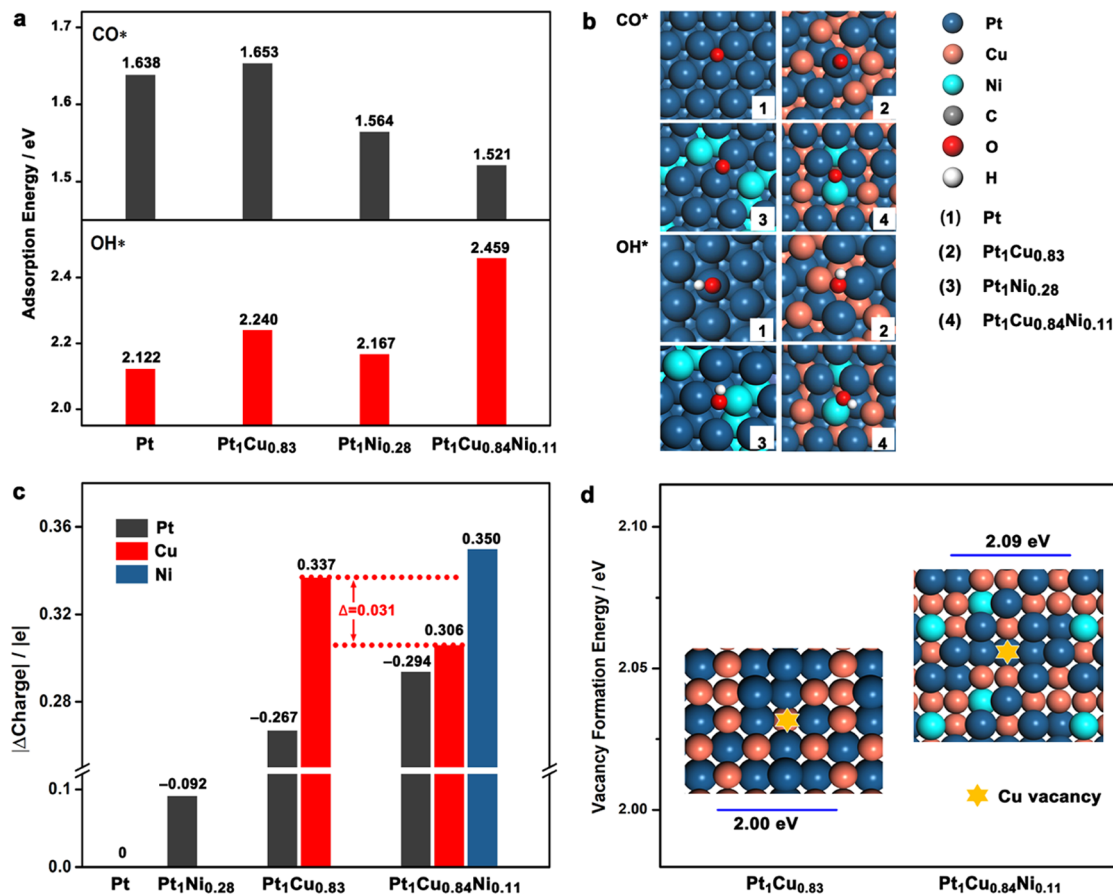


**Figure 4.** DFT calculation results. (a) Adsorption energies of CO\* and OH\* on the surface of Pt, Pt<sub>1</sub>Cu<sub>0.83</sub>, Pt<sub>1</sub>Ni<sub>0.28</sub>, and Pt<sub>1</sub>Cu<sub>0.84</sub>Ni<sub>0.11</sub>. (b) Configurations of CO\* and OH\* on the respective metal surfaces. (c) Bader charge analysis. Bars represent the absolute values of the charges (|Δcharge|) at the outmost metal atoms of the catalysts. Negative values: metal atoms gain electrons. Positive values: metal atoms lose electrons. (d) Formation energy of a Cu vacancy on a Pt<sub>1</sub>Cu<sub>0.83</sub> and Pt<sub>1</sub>Cu<sub>0.84</sub>Ni<sub>0.11</sub> surface. Inset shows the position of the Cu vacancy.

oxidation kinetics. To better correlate the catalytic activity with the alloy compositions, we placed all of the activity values of the catalysts in a ternary diagram (Figure 2d). The three axes of the diagram indicate the alloy compositions, and the colors of the data points indicate the specific activity values. The highest activity appears in the interior area of the diagram rather than on the edges, which clearly illustrates the advantages of the Pt–Cu–Ni ternary alloy nanowires over the binary alloy counterparts in catalyzing the MOR. It is worth noting that the specific and mass activities of the Pt<sub>1</sub>Cu<sub>0.84</sub>Ni<sub>0.11</sub> catalyst are 7.6 and 4.4 times greater than those of the commercial Pt/C, respectively, which places it in a leading position among all catalysts reported to date (Table S8).<sup>12,15,20,22,25,29,51,52</sup>

The catalytic stability was further examined by the chronoamperometric *i*–*t* test (Figures 2e and S14). After the potential was maintained at 0.8 V for 5000 s, the current density of the Pt<sub>1</sub>Cu<sub>0.84</sub>Ni<sub>0.11</sub> ternary alloy nanowires was 0.602 mA cm<sup>−2</sup>, 5.7 times greater than that of the commercial Pt/C (0.106 mA cm<sup>−2</sup>). Remarkably, the current density of the Pt<sub>1</sub>Cu<sub>0.84</sub>Ni<sub>0.11</sub> ternary alloy nanowires was substantially higher than those of the Pt–M (M = Cu, Ni) binary alloy nanowires after the long-term catalysis. The reasons for the high catalytic stability of the Pt–Cu–Ni ternary alloy nanowires could be twofold. First, the nanowires retained the one-dimensional morphology without significant agglomeration during the catalysis (Figure S15). Second, the dissolution of the major

non-noble metal, i.e., Cu, from the ternary alloy nanowires was alleviated compared with the binary alloy nanowires (Figures 2f and S16 and Table S9). As revealed by ICP-MS, the Pt<sub>1</sub>Cu<sub>0.83</sub> binary alloy nanowires lost 63% of its Cu after 20 000 s of the *i*–*t* test. In clear contrast, the loss of Cu from the Pt<sub>1</sub>Cu<sub>0.84</sub>Ni<sub>0.11</sub> ternary alloy nanowires was only 34% under the same conditions, albeit a similar Cu/Pt ratio in the nanowires. EDS elemental mapping further confirms that the Pt–Cu–Ni ternary alloy compositions distribute homogeneously in the nanowires after the *i*–*t* test, without showing elemental segregations (Figure S17). Therefore, the corrosion of Cu in the ternary alloy nanowires has been significantly suppressed under the high potential in an acidic electrolyte, which contributes to the improved catalytic stability.

**Mechanisms.** To understand the multimetallic interplay, we inspected the electronic properties of the Pt–Cu–Ni ternary alloy nanowires in comparison with those of the Pt–M (M = Cu, Ni) binary alloy nanowires and the monometallic Pt/C (Figure 3). The oxidation state of Pt was analyzed by X-ray photoelectron spectroscopy (XPS) (Figure 3a). The Pt 4f spectra can be fitted by two sets of spin–orbit split 4f<sub>7/2</sub> and 4f<sub>5/2</sub> components, with the 4f<sub>7/2</sub> component at ~71 and ~72 eV corresponding to the Pt(0) and Pt(II) species, respectively. All of the Pt(0) peaks of the Pt<sub>1</sub>Cu<sub>0.83</sub>, Pt<sub>1</sub>Ni<sub>0.28</sub>, and Pt<sub>1</sub>Cu<sub>0.84</sub>Ni<sub>0.11</sub> nanowires shift to lower binding energies than that of the Pt/C, suggesting an electron transfer from the non-noble metals to Pt. Among all catalysts investigated, the

Pt<sub>1</sub>Cu<sub>0.84</sub>Ni<sub>0.11</sub> nanowires show the most notable shift of the Pt(0) peak. Therefore, the Pt sites in the Pt–Cu–Ni ternary alloy nanowires are more electron rich than Pt in both the Pt–M (M = Cu, Ni) binary alloy nanowires. To gain a full picture of the electron transfer, we further examined the XPS spectra of the non-noble metals (Figures S18 and S19 and Table S10). The Ni 2p peaks of the Pt<sub>1</sub>Cu<sub>0.84</sub>Ni<sub>0.11</sub> nanowires shift to higher binding energies than those of the Pt<sub>1</sub>Ni<sub>0.28</sub> nanowires, while the positions of the Cu 2p peaks are almost unchanged compared with the Pt<sub>1</sub>Cu<sub>0.83</sub> nanowires. It indicates that Ni behaves as a stronger electron donor than Cu, albeit its low fraction in the alloy nanowires. The electronic coupling between the Pt–Cu–Ni components may significantly influence the catalytic properties of the nanowires.

The electronic properties of the catalysts could also be examined by using CO as a probe. As revealed by the CO stripping voltammetry (Figure 3b), the oxidation of CO from all alloy nanowires shifts to low potentials applied compared with the monometallic Pt/C. In particular, the CO oxidation on the Pt<sub>1</sub>Cu<sub>0.84</sub>Ni<sub>0.11</sub> ternary alloy nanowires occurs at the lowest potential, which is in line with the highest charge density at the Pt sites as inferred from the XPS data. It is also inferred that the poisonous intermediate of CO could be removed most easily from the Pt<sub>1</sub>Cu<sub>0.84</sub>Ni<sub>0.11</sub> ternary alloy nanowires in the MOR, contributing to the best reaction kinetics as observed experimentally.

We further conducted DFT calculations to rationalize the Pt–Cu–Ni multimetallic interplay in the MOR (Figure 4). Four models were constructed to simulate the catalysts with different compositions: Pt, Pt<sub>1</sub>Cu<sub>0.83</sub>, Pt<sub>1</sub>Ni<sub>0.28</sub>, and Pt<sub>1</sub>Cu<sub>0.84</sub>Ni<sub>0.11</sub>. We first calculated the adsorption energies of \*CO and \*OH, two widely accepted descriptors for the MOR, on these surfaces (Figure 4a).<sup>3</sup> Pt<sub>1</sub>Cu<sub>0.84</sub>Ni<sub>0.11</sub> is predicted to be the best catalyst for the MOR because it possesses the lowest adsorption energy of \*CO and the highest adsorption energy of \*OH, both being favorable for accelerating the methanol oxidation kinetics. The changes in the binding energy are also reflected from the various binding modes of \*CO and \*OH according to the DFT calculations (Figure 4b). Specifically, \*CO adsorbs on Pt, Pt<sub>1</sub>Cu<sub>0.83</sub>, Pt<sub>1</sub>Ni<sub>0.28</sub>, and Pt<sub>1</sub>Cu<sub>0.84</sub>Ni<sub>0.11</sub> at Pt<sub>3</sub> fcc hollow site, Pt top site, Pt–Pt bridge site, and Pt<sub>2</sub>Ni fcc hollow site, respectively, and \*OH adsorbs on these catalysts at the Pt top site, Pt–Cu bridge site, Pt–Ni bridge site, and Pt–Ni bridge site, respectively. The multimetallic alloying provides rich sites for the adsorption of \*CO and \*OH with diverse local environments, allowing effective tuning of their adsorption energies (Figure 4a). Although the Pt–Cu alloying leads to an unfavorable increase in the \*CO adsorption energy, the Pt–Ni alloying significantly reduces this value. The ternary alloying of Pt–Cu–Ni, interestingly, can reduce the \*CO adsorption energy to a level that is much lower than both the binary alloys, consistent with the CO stripping results (Figure 3b). On the other hand, both the Pt–Cu and the Pt–Ni alloys possess a high \*OH adsorption energy. Notably, the ternary alloying of Pt–Cu–Ni can increase the \*OH adsorption to a level that is significantly higher than both the binary alloys. The calculated adsorption energies of \*CO and \*OH well explained the superiority of the Pt–Cu–Ni ternary alloy nanowires over the Pt–M (M = Cu, Ni) binary alloy nanowires in catalyzing the MOR. The ternary components function collectively to afford distinctive catalytic properties.

The catalytic performance of the alloy catalysts should be closely correlated with the oxidation states of the metal atoms, characterized by the atomic charges. Therefore, we carried out Barder analysis to assign the charges of the metal atoms on the outmost surface of the catalysts (Figure 4c and Table S11). For all of the alloys, an electron transfer from Cu/Ni to Pt was observed. The values of the negative charges ( $q$ ) at the Pt sites increase in the order of Pt(0) < Pt<sub>1</sub>Ni<sub>0.28</sub> (-0.092 e) < Pt<sub>1</sub>Cu<sub>0.83</sub> (-0.267 e) < Pt<sub>1</sub>Cu<sub>0.84</sub>Ni<sub>0.11</sub> (-0.294 e) (in term of the absolute values), suggesting that Pt is more reduced in this order. This trend is generally consistent with the XPS results within the accuracy and uncertainty of both experiment and theory (Figure 3a). Meanwhile, the charge separations agree well with the \*OH adsorption energies (Figure 4a), which demonstrates the critical role of the electron transfer in modulating the adsorption energy of the reactants and their intermediates. Considering that the electronegativity values of Ni and Cu are very close, we expect that the reduction of Pt is caused by the electron transfer from both Cu and Ni. The positive charge at the Cu site of the Pt<sub>1</sub>Cu<sub>0.84</sub>Ni<sub>0.11</sub> alloy surface is 0.306 e, which is 0.031 e lower than that in the Pt<sub>1</sub>Cu<sub>0.83</sub> alloy (Figure 4c). Such a mismatch apparently results from the electron compensation by Ni: the electron transfer from Ni to Pt leads to a positive charge (0.350 e) at the Ni site, which suppresses the electron donation from Cu, leading to less oxidized Cu sites. Thus, the mutual electron coupling among the ternary components of the Pt–Cu–Ni alloy finely tunes the oxidation states of the metal sites and accounts for their enhanced catalytic activities.

The less oxidized Cu sites on the Pt<sub>1</sub>Cu<sub>0.84</sub>Ni<sub>0.11</sub> surface may explain the fact that Cu in the ternary alloy nanowires is less prone to oxidation or erosion during electrocatalysis. To verify this assumption, we calculated the formation energies of a Cu vacancy on Pt<sub>1</sub>Cu<sub>0.83</sub> and Pt<sub>1</sub>Cu<sub>0.84</sub>Ni<sub>0.11</sub> surfaces, and the results are shown in Figure 4d. Compared with the binary alloy of Pt<sub>1</sub>Cu<sub>0.83</sub>, the ternary alloy of Pt<sub>1</sub>Cu<sub>0.84</sub>Ni<sub>0.11</sub> exhibits an increase in the formation energy of the Cu vacancy by 0.09 eV, which refers to stronger resistance of Cu solvation into the electrolyte. Therefore, the mutual electron coupling in Pt<sub>1</sub>Cu<sub>0.84</sub>Ni<sub>0.11</sub> ternary alloy also contributes to the improved stability of the nanowires in the MOR.

## CONCLUSIONS

In summary, we have demonstrated the successful synthesis of Pt–Cu–Ni ternary alloy nanowires in a controllable manner and revealed an interesting multimetallic interplay that enabled us to achieve highly improved activity and stability in the electrocatalytic MOR. Our synthesis relies on the controlled coreduction of the different metal salts at a comparable rate by introducing an electroless plating mechanism into a wet-chemical system. The resulting Pt–Cu–Ni ternary alloy nanowires showed excellent catalytic activity and stability in the MOR, superior to both the Pt–Cu and the Pt–Ni binary alloy nanowires. Experiments and DFT calculations confirm that electronic coupling occurs among the Pt–Cu–Ni ternary alloy components: Pt becomes significantly electron rich by gaining electrons from both Cu and Ni, and the Cu–Pt electron transfer is suppressed by the alloying of Ni. These electronic coupling effects significantly alter the adsorption energies of the reactants and intermediates in the MOR, contributing to the significantly enhanced reaction kinetics. The electronic coupling effects also suppressed the leaching of Cu, the primary non-noble metal, from the ternary alloy

nanowires, leading to improved catalytic stability. All of these facts confirm the critical role of multimetallic interplay in enhancing the performance of the catalysts. We expect that this effect may exist in many other metal-nanoparticle-based catalytic systems for a broad range of reactions, which helps push the performance of catalysts to high levels for improved viability in practical applications.

## ■ ASSOCIATED CONTENT

### SI Supporting Information

The Supporting Information is available free of charge at <https://pubs.acs.org/doi/10.1021/acsaem.1c00952>.

Full experimental details; additional TEM images; ICP-MS; XPS; DFT calculations; electrocatalytic results; and comparison of the catalytic activity with literature-reported values ([PDF](#))

## ■ AUTHOR INFORMATION

### Corresponding Authors

Tao Cheng – Institute of Functional Nano & Soft Materials (FUNSOM), Jiangsu Key Laboratory for Carbon-Based Functional Materials & Devices, Joint International Research Laboratory of Carbon-Based Functional Materials and Devices, Soochow University, Suzhou, Jiangsu 215123, China; [orcid.org/0000-0003-4830-177X](https://orcid.org/0000-0003-4830-177X); Email: [tcheng@suda.edu.cn](mailto:tcheng@suda.edu.cn)

Chuanbo Gao – Center for Materials Chemistry, Frontier Institute of Science and Technology, and State Key Laboratory of Multiphase Flow in Power Engineering, Xi'an Jiaotong University, Xi'an, Shaanxi 710054, China; [orcid.org/0000-0003-3429-3473](https://orcid.org/0000-0003-3429-3473); Email: [gaochuanbo@mail.xjtu.edu.cn](mailto:gaochuanbo@mail.xjtu.edu.cn)

### Authors

Zhixue Zhang – Center for Materials Chemistry, Frontier Institute of Science and Technology, and State Key Laboratory of Multiphase Flow in Power Engineering, Xi'an Jiaotong University, Xi'an, Shaanxi 710054, China

Miao Xie – Institute of Functional Nano & Soft Materials (FUNSOM), Jiangsu Key Laboratory for Carbon-Based Functional Materials & Devices, Joint International Research Laboratory of Carbon-Based Functional Materials and Devices, Soochow University, Suzhou, Jiangsu 215123, China; [orcid.org/0000-0002-9797-1449](https://orcid.org/0000-0002-9797-1449)

Zhaojun Liu – Center for Materials Chemistry, Frontier Institute of Science and Technology, and State Key Laboratory of Multiphase Flow in Power Engineering, Xi'an Jiaotong University, Xi'an, Shaanxi 710054, China

Yiming Lu – Institute of Functional Nano & Soft Materials (FUNSOM), Jiangsu Key Laboratory for Carbon-Based Functional Materials & Devices, Joint International Research Laboratory of Carbon-Based Functional Materials and Devices, Soochow University, Suzhou, Jiangsu 215123, China

Shumeng Zhang – Center for Materials Chemistry, Frontier Institute of Science and Technology, and State Key Laboratory of Multiphase Flow in Power Engineering, Xi'an Jiaotong University, Xi'an, Shaanxi 710054, China

Moxuan Liu – Center for Materials Chemistry, Frontier Institute of Science and Technology, and State Key Laboratory of Multiphase Flow in Power Engineering, Xi'an Jiaotong University, Xi'an, Shaanxi 710054, China

Kai Liu – Center for Materials Chemistry, Frontier Institute of Science and Technology, and State Key Laboratory of Multiphase Flow in Power Engineering, Xi'an Jiaotong University, Xi'an, Shaanxi 710054, China

Complete contact information is available at: <https://pubs.acs.org/10.1021/acsaem.1c00952>

### Author Contributions

§Z.Z. and M.X. contributed equally to this work.

### Notes

The authors declare no competing financial interest.

## ■ ACKNOWLEDGMENTS

C.G. acknowledges the support by the National Natural Science Foundation of China (22071191 and 21671156), the Key Scientific and Technological Innovation Team of Shaanxi Province (2020TD-001), the Fundamental Research Funds for the Central Universities, and the World-Class Universities (Disciplines) and the Characteristic Development Guidance Funds for the Central Universities. The work of T.C. was supported by the National Natural Science Foundation of China (21903058), the Natural Science Foundation of Jiangsu Province (BK20190810), Jiangsu Province High-Level Talents (JNHB-106), Collaborative Innovation Center of Suzhou Nano Science & Technology, and the 111 Project. K.L. acknowledges the support by the Project funded by China Postdoctoral Science Foundation (2019TQ0249). The authors thank the Instrument Analysis Center of Xi'an Jiaotong University for partial assistance with the HRTEM and XPS measurements.

## ■ REFERENCES

- (1) Tong, Y.; Yan, X.; Liang, J.; Dou, S. X. Metal-Based Electrocatalysts for Methanol Electro-Oxidation: Progress, Opportunities, and Challenges. *Small* **2021**, *17*, No. 1904126.
- (2) Lyu, F.; Cao, M.; Mahsud, A.; Zhang, Q. Interfacial Engineering of Noble Metals for Electrocatalytic Methanol and Ethanol Oxidation. *J. Mater. Chem. A* **2020**, *8*, 15445–15457.
- (3) Ferrin, P.; Mavrikakis, M. Structure Sensitivity of Methanol Electrooxidation on Transition Metals. *J. Am. Chem. Soc.* **2009**, *131*, 14381–14389.
- (4) Neurock, M.; Janik, M.; Wieckowski, A. A First Principles Comparison of the Mechanism and Site Requirements for the Electrocatalytic Oxidation of Methanol and Formic Acid over Pt. *Faraday Discuss.* **2009**, *140*, 363–378.
- (5) Chung, D. Y.; Lee, K.-J.; Sung, Y. E. Methanol Electro-Oxidation on the Pt Surface: Revisiting the Cyclic Voltammetry Interpretation. *J. Phys. Chem. C* **2016**, *120*, 9028–9035.
- (6) Tang, Q.; Chen, F.; Jin, T.; Guo, L.; Wang, Q.; Liu, H. Alloying in Inverse CeO<sub>2</sub>/Pd Nanoparticles to Enhance the Electrocatalytic Activity for the Formate Oxidation Reaction. *J. Mater. Chem. A* **2019**, *7*, 22996–23007.
- (7) Wang, Q.; Chen, F.; Guo, L.; Jin, T.; Liu, H.; Wang, X.; Gong, X.; Liu, Y. Nanoalloying Effects on the Catalytic Activity of the Formate Oxidation Reaction over AgPd and AgCuPd Aerogels. *J. Mater. Chem. A* **2019**, *7*, 16122–16135.
- (8) Guo, L.; Chen, F.; Jin, T.; Liu, H.; Zhang, N.; Jin, Y.; Wang, Q.; Tang, Q.; Pan, B. Surface Reconstruction of AgPd Nanoalloy Particles During the Electrocatalytic Formate Oxidation Reaction. *Nanoscale* **2020**, *12*, 3469–3481.
- (9) Wang, J.; Chen, F.; Jin, Y.; Guo, L.; Gong, X.; Wang, X.; Johnston, R. L. In Situ High-Potential-Driven Surface Restructuring of Ternary AgPd-Pt<sub>dilute</sub> Aerogels with Record-High Performance Improvement for Formate Oxidation Electrocatalysis. *Nanoscale* **2019**, *11*, 14174–14185.

- (10) Farmand, M.; Landers, A. T.; Lin, J. C.; Feaster, J. T.; Beeman, J. W.; Ye, Y.; Clark, E. L.; Higgins, D.; Yano, J.; Davis, R. C.; Mehta, A.; Jaramillo, T. F.; Hahn, C.; Drisdell, W. S. Electrochemical Flow Cell Enabling Operando Probing of Electrocatalyst Surfaces by X-Ray Spectroscopy and Diffraction. *Phys. Chem. Chem. Phys.* **2019**, *21*, 5402–5408.
- (11) Petrii, O. A. Pt–Ru Electrocatalysts for Fuel Cells: A Representative Review. *J. Solid State Electrochem.* **2008**, *12*, 609–642.
- (12) Zhao, W.-Y.; Ni, B.; Yuan, Q.; He, P.-L.; Gong, Y.; Gu, L.; Wang, X. Highly Active and Durable Pt<sub>72</sub>Ru<sub>28</sub> porous Nanoalloy Assembled with Sub-4.0 nm Particles for Methanol Oxidation. *Adv. Energy Mater.* **2017**, *7*, No. 1601593.
- (13) Huang, L.; Zhang, X.; Wang, Q.; Han, Y.; Fang, Y.; Dong, S. Shape-Control of Pt–Ru Nanocrystals: Tuning Surface Structure for Enhanced Electrocatalytic Methanol Oxidation. *J. Am. Chem. Soc.* **2018**, *140*, 1142–1147.
- (14) Zhang, J.; Qu, X.; Han, Y.; Shen, L.; Yin, S.; Li, G.; Jiang, Y.; Sun, S. Engineering PtRu Bimetallic Nanoparticles with Adjustable Alloying Degree for Methanol Electrooxidation: Enhanced Catalytic Performance. *Appl. Catal., B* **2020**, *263*, No. 118345.
- (15) Zhang, W.; Yang, Y.; Huang, B.; Lv, F.; Wang, K.; Li, N.; Luo, M.; Chao, Y.; Li, Y.; Sun, Y.; Xu, Z.; Qin, Y.; Yang, W.; Zhou, J.; Du, Y.; Su, D.; Guo, S. Ultrathin PtNiM (M = Rh, Os, and Ir) Nanowires as Efficient Fuel Oxidation Electrocatalytic Materials. *Adv. Mater.* **2019**, *31*, No. e1805833.
- (16) Xue, S.; Deng, W.; Yang, F.; Yang, J.; Amiinu, I. S.; He, D.; Tang, H.; Mu, S. Hexapod PtRuCu Nanocrystalline Alloy for Highly Efficient and Stable Methanol Oxidation. *ACS Catal.* **2018**, *8*, 7578–7584.
- (17) Li, H.; Pan, Y.; Zhang, D.; Han, Y.; Wang, Z.; Qin, Y.; Lin, S.; Wu, X.; Zhao, H.; Lai, J.; Huang, B.; Wang, L. Surface Oxygen-Mediated Ultrathin PtRuM (Ni, Fe, and Co) Nanowires Boosting Methanol Oxidation Reaction. *J. Mater. Chem. A* **2020**, *8*, 2323–2330.
- (18) Qin, Y.; Luo, M.; Sun, Y.; Li, C.; Huang, B.; Yang, Y.; Li, Y.; Wang, L.; Guo, S. Intermetallic *hcp*-PtBi/*fcc*-Pt Core/Shell Nanoplates Enable Efficient Bifunctional Oxygen Reduction and Methanol Oxidation Electrocatalysis. *ACS Catal.* **2018**, *8*, 5581–5590.
- (19) Rossmeisl, J.; Ferrin, P.; Tritsaris, G. A.; Nilekar, A. U.; Koh, S.; Bae, S. E.; Brankovic, S. R.; Strasser, P.; Mavrikakis, M. Bifunctional Anode Catalysts for Direct Methanol Fuel Cells. *Energy Environ. Sci.* **2012**, *5*, 8335–8342.
- (20) Luo, S.; Shen, P. K. Concave Platinum–Copper Octopod Nanoframes Bounded with Multiple High-Index Facets for Efficient Electrooxidation Catalysis. *ACS Nano* **2017**, *11*, 11946–11953.
- (21) Zhang, Z.; Luo, Z.; Chen, B.; Wei, C.; Zhao, J.; Chen, J.; Zhang, X.; Lai, Z.; Fan, Z.; Tan, C.; Zhao, M.; Lu, Q.; Li, B.; Zong, Y.; Yan, C.; Wang, G.; Xu, Z. J.; Zhang, H. One-Pot Synthesis of Highly Anisotropic Five-Fold-Twinned PtCu Nanoframes Used as a Bifunctional Electrocatalyst for Oxygen Reduction and Methanol Oxidation. *Adv. Mater.* **2016**, *28*, 8712–8717.
- (22) Li, H.-H.; Fu, Q.-Q.; Xu, L.; Ma, S.-Y.; Zheng, Y.-R.; Liu, X.-J.; Yu, S.-H. Highly Crystalline PtCu Nanotubes with Three Dimensional Molecular Accessible and Restructured Surface for Efficient Catalysis. *Energy Environ. Sci.* **2017**, *10*, 1751–1756.
- (23) Huang, L.; Zhang, X.; Han, Y.; Wang, Q.; Fang, Y.; Dong, S. High-Index Facets Bounded Platinum–Lead Concave Nanocubes with Enhanced Electrocatalytic Properties. *Chem. Mater.* **2017**, *29*, 4557–4562.
- (24) Zhang, Y.; Huang, B.; Shao, Q.; Feng, Y.; Xiong, L.; Peng, Y.; Huang, X. Defect Engineering of Palladium-Tin Nanowires Enables Efficient Electrocatalysts for Fuel Cell Reactions. *Nano Lett.* **2019**, *19*, 6894–6903.
- (25) Feng, Q.; Zhao, S.; He, D.; Tian, S.; Gu, L.; Wen, X.; Chen, C.; Peng, Q.; Wang, D.; Li, Y. Strain Engineering to Enhance the Electrooxidation Performance of Atomic-Layer Pt on Intermetallic Pt<sub>3</sub>Ga. *J. Am. Chem. Soc.* **2018**, *140*, 2773–2776.
- (26) Wang, L.; Tian, X. L.; Xu, Y.; Zaman, S.; Qi, K.; Liu, H.; Xia, B. Y. Engineering One-Dimensional and Hierarchical PtFe Alloy Assemblies Towards Durable Methanol Electrooxidation. *J. Mater. Chem. A* **2019**, *7*, 13090–13095.
- (27) Xu, Y.; Cui, X.; Wei, S.; Zhang, Q.; Gu, L.; Meng, F.; Fan, J.; Zheng, W. Highly Active Zigzag-Like Pt-Zn Alloy Nanowires with High-Index Facets for Alcohol Electrooxidation. *Nano Res.* **2019**, *12*, 1173–1179.
- (28) Xia, B. Y.; Wu, H. B.; Li, N.; Yan, Y.; Lou, X. W.; Wang, X. One-Pot Synthesis of Pt-Co Alloy Nanowire Assemblies with Tunable Composition and Enhanced Electrocatalytic Properties. *Angew. Chem., Int. Ed.* **2015**, *54*, 3797–3801.
- (29) Yang, P.; Yuan, X.; Hu, H.; Liu, Y.; Zheng, H.; Yang, D.; Chen, L.; Cao, M.; Xu, Y.; Min, Y.; Li, Y.; Zhang, Q. Solvothermal Synthesis of Alloyed PtNi Colloidal Nanocrystal Clusters (CNCs) with Enhanced Catalytic Activity for Methanol Oxidation. *Adv. Funct. Mater.* **2018**, *28*, No. 1704774.
- (30) Zhao, Z.; Feng, M.; Zhou, J.; Liu, Z.; Li, M.; Fan, Z.; Tsen, O.; Miao, J.; Duan, X.; Huang, Y. Composition Tunable Ternary Pt-Ni-Co Octahedra for Optimized Oxygen Reduction Activity. *Chem. Commun.* **2016**, *52*, 11215–11218.
- (31) Yao, Y.; Huang, Z.; Xie, P.; Lacey, S. D.; Jacob, R. J.; Xie, H.; Chen, F.; Nie, A.; Pu, T.; Rehwoldt, M.; Yu, D.; Zachariah, M. R.; Wang, C.; Shahbazian-Yassar, R.; Li, J.; Hu, L. Carbothermal Shock Synthesis of High-Entropy-Alloy Nanoparticles. *Science* **2018**, *359*, 1489–1494.
- (32) Kobayashi, H.; Kusada, K.; Kitagawa, H. Creation of Novel Solid-Solution Alloy Nanoparticles on the Basis of Density-of-States Engineering by Interelement Fusion. *Acc. Chem. Res.* **2015**, *48*, 1551–1559.
- (33) Gilroy, K. D.; Ruditskiy, A.; Peng, H.-C.; Qin, D.; Xia, Y. Bimetallic Nanocrystals: Syntheses, Properties, and Applications. *Chem. Rev.* **2016**, *116*, 10414–10472.
- (34) Skrabalak, S. E. Mashing up Metals with Carbothermal Shock. *Science* **2018**, *359*, 1467.
- (35) Zeng, R.; Yang, Y.; Shen, T.; Wang, H.; Xiong, Y.; Zhu, J.; Wang, D.; Abruna, H. D. Methanol Oxidation Using Ternary Ordered Intermetallic Electrocatalysts: A Dems Study. *ACS Catal.* **2020**, *10*, 770–776.
- (36) Zhang, C.; Sandorf, W.; Peng, Z. Octahedral Pt<sub>2</sub>CuNi Uniform Alloy Nanoparticle Catalyst with High Activity and Promising Stability for Oxygen Reduction Reaction. *ACS Catal.* **2015**, *5*, 2296–2300.
- (37) Wu, D.; Zhang, W.; Lin, A.; Cheng, D. Low Pt-Content Ternary PtNiCu Nanoparticles with Hollow Interiors and Accessible Surfaces as Enhanced Multifunctional Electrocatalysts. *ACS Appl. Mater. Interfaces* **2020**, *12*, 9600–9608.
- (38) Arán-Ais, R. M.; Dionigi, F.; Merzdorf, T.; Gocyla, M.; Heggen, M.; Dunin-Borkowski, R. E.; Gliech, M.; Solla-Gullon, J.; Herrero, E.; Feliu, J. M.; Strasser, P. Elemental Anisotropic Growth and Atomic-Scale Structure of Shape-Controlled Octahedral Pt-Ni-Co Alloy Nanocatalysts. *Nano Lett.* **2015**, *15*, 7473–7480.
- (39) Park, J.; Kanti Kabiraz, M.; Kwon, H.; Park, S.; Baik, H.; Choi, S. I.; Lee, K. Radially Phase Segregated PtCu@PtCuNi Dendrite@Frame Nanocatalyst for the Oxygen Reduction Reaction. *ACS Nano* **2017**, *11*, 10844–10851.
- (40) Huang, J.; Liu, Y.; Xu, M.; Wan, C.; Liu, H.; Li, M.; Huang, Z.; Duan, X.; Pan, X.; Huang, Y. PtCuNi Tetrahedra Catalysts with Tailored Surfaces for Efficient Alcohol Oxidation. *Nano Lett.* **2019**, *19*, 5431–5436.
- (41) Gao, D.; Yang, S.; Xi, L.; Risch, M.; Song, L.; Lv, Y.; Li, C.; Li, C.; Chen, G. External and Internal Interface-Controlled Trimetallic PtCuNi Nanoframes with High Defect Density for Enhanced Electrooxidation of Liquid Fuels. *Chem. Mater.* **2020**, *32*, 1581–1594.
- (42) Zhang, P.; Dai, X.; Zhang, X.; Chen, Z.; Yang, Y.; Sun, H.; Wang, X.; Wang, H.; Wang, M.; Su, H.; Li, D.; Li, X.; Qin, Y. One-Pot Synthesis of Ternary Pt–Ni–Cu Nanocrystals with High Catalytic Performance. *Chem. Mater.* **2015**, *27*, 6402–6410.
- (43) Huang, X. Q.; Zhao, Z. P.; Cao, L.; Chen, Y.; Zhu, E. B.; Lin, Z. Y.; Li, M. F.; Yan, A. M.; Zettl, A.; Wang, Y. M.; Duan, X. F.; Mueller, T.; Huang, Y. High-Performance Transition Metal-Doped Pt<sub>3</sub>Ni

Octahedra for Oxygen Reduction Reaction. *Science* **2015**, *348*, 1230–1234.

(44) Cao, L.; Zhao, Z.; Liu, Z.; Gao, W.; Dai, S.; Gha, J.; Xue, W.; Sun, H.; Duan, X.; Pan, X.; Mueller, T.; Huang, Y. Differential Surface Elemental Distribution Leads to Significantly Enhanced Stability of PtNi-Based ORR Catalysts. *Matter* **2019**, *1*, 1567–1580.

(45) Kwon, T.; Jun, M.; Kim, H. Y.; Oh, A.; Park, J.; Baik, H.; Joo, S. H.; Lee, K. Vertex-Reinforced PtCuCo Ternary Nanoframes as Efficient and Stable Electrocatalysts for the Oxygen Reduction Reaction and the Methanol Oxidation Reaction. *Adv. Funct. Mater.* **2018**, *28*, No. 1706440.

(46) Lim, J.; Shin, H.; Kim, M.; Lee, H.; Lee, K.-S.; Kwon, Y.; Song, D.; Oh, S.; Kim, H.; Cho, E. Ga-Doped Pt–Ni Octahedral Nanoparticles as a Highly Active and Durable Electrocatalyst for Oxygen Reduction Reaction. *Nano Lett.* **2018**, *18*, 2450–2458.

(47) Liu, Z.; Qi, J.; Liu, M.; Zhang, S.; Fan, Q.; Liu, H.; Liu, K.; Zheng, H.; Yin, Y.; Gao, C. Aqueous Synthesis of Ultrathin Platinum/Non-Noble Metal Alloy Nanowires for Enhanced Hydrogen Evolution Activity. *Angew. Chem., Int. Ed.* **2018**, *57*, 11678–11682.

(48) Soldo, Y.; Sibert, E.; Tourillon, G.; Hazemann, J. L.; Lévy, J. P.; Aberdam, D.; Faure, R.; Durand, R. In Situ X-Ray Absorption Spectroscopy Study of Copper under Potential Deposition on Pt(111): Role of the Anions on the Cu Structural Arrangement. *Electrochim. Acta* **2002**, *47*, 3081–3091.

(49) Guo, L.; Huang, L.-B.; Jiang, W.-J.; Wei, Z.-D.; Wan, L.-J.; Hu, J.-S. Tuning the Branches and Composition of PtCu Nanodendrites through Underpotential Deposition of Cu Towards Advanced Electrocatalytic Activity. *J. Mater. Chem. A* **2017**, *5*, 9014–9021.

(50) Jerkiewicz, G.; Perreault, F.; Radovic-Hrapovic, Z. Effect of Temperature Variation on the Under-Potential Deposition of Copper on Pt(111) in Aqueous  $\text{H}_2\text{SO}_4$ . *J. Phys. Chem. C* **2009**, *113*, 12309–12316.

(51) Liu, H.; Liu, K.; Zhong, P.; Qi, J.; Bian, J.; Fan, Q.; Ren, K.; Zheng, H.; Han, L.; Yin, Y.; Gao, C. Ultrathin Pt–Ag Alloy Nanotubes with Regular Nanopores for Enhanced Electrocatalytic Activity. *Chem. Mater.* **2018**, *30*, 7744–7751.

(52) Luo, X.; Liu, C.; Wang, X.; Shao, Q.; Pi, Y.; Zhu, T.; Li, Y.; Huang, X. Spin Regulation on 2d Pd–Fe–Pt Nanomeshes Promotes Fuel Electrooxidations. *Nano Lett.* **2020**, *20*, 1967–1973.